



Interactions of variously coated gold and silver nanoparticles with a bis(triarylborane) photodynamic therapy (PDT)-dye; their cellular uptake, cytotoxicity and photo-activity

ISABELA DRAŠKOVIĆ¹⁺
IVANA FABIJANIĆ²⁺
MATTHIAS FERGER³
TODD B. MARDER³
DRAGOMIRA MAJHEN^{1*}
IVO PIANTANIDA^{2*}

¹ Laboratory for Cell Biology and Signalling, Division of Molecular Biology, Ruđer Bošković Institute, Zagreb, Croatia

² Laboratory for Biomolecular Interactions and Spectroscopy, Division of Organic Chemistry and Biochemistry, Ruđer Bošković Institute, Zagreb, Croatia

³ Institut für Anorganische Chemie, and Institute for Sustainable Chemistry & Catalysis with Boron, Julius-Maximilians-Universität Würzburg, Würzburg, Germany

*Equal contribution

*Correspondence:

Dragomira Majhen
E-mail address: Dragomira.Majhen@irb.hr
Ivo Piantanida
E-mail address: pianta@irb.hr

Keywords: silver nanoparticles; gold nanoparticles; triarylborane dye; cellular uptake; bioimaging; drug-delivery

Received October 27, 2022
Revised December 22, 2022
Accepted January 5, 2023

Abstract

Background and purpose: Diethynylarene-linked bis(triarylborane) tetracations can be used as probes for fluorimetric and Raman sensing of biomacromolecules, as well as promising theragnostic agents. Among them, bis(triarylborane) fluorophore (TAB3), when bonded to Ag nanoparticles (NP), stood out with specific properties such as Raman signal enhancement of the TAB3 dye in a cuvette. However, TAB3 dye - nanoparticle composites have not been studied in biological systems. For this reason, questions arose as to whether different types of metal nanoparticles (Au or Ag-based) with different coatings (negatively charged citrate or neutral PVP) could be efficiently stained with the TAB3 dye in a cuvette. The aim of this research was to examine Au and Ag nanoparticles of similar size (20–25 nm) with different stabilizers for their cellular uptake, cytotoxicity in the dark and under visible light radiation, to characterize the interactions of nanoparticles with the TAB3 fluorophore, and to study NP-TAB3 composites in cells, evaluate their intracellular staining, as well as possible photoinduced release and biological activity.

Materials and methods: The binding constants of Au- and Ag- based nanoparticles with TAB3 were determined by fluorimetric titrations. The cytotoxic effect of NPs was determined by the survival of A549 cells (MTT assay). Cellular uptake of both NP and NP-TAB3 composites were performed by live cell imaging experiments.

Results: The Au- or Ag-based NPs with different coatings bind to the TAB3 with high affinity. These NPs, as well as TAB3-NP complexes, efficiently enter living human cells, accumulating in cytoplasm with no apparent selectivity for a particular organelle. Even prolonged 3-day treatment with the NPs studied did not show any toxic effect on the cells. Bioimaging studies in cells revealed that the TAB3-NP complex does not intracellularly dissociate; the previously reported photo-bioactivity of TAB3 is completely inhibited by binding to NPs.

Conclusion: Au- and Ag NPs were non-covalently stained by TAB3, irrespective of the different coatings, with similar binding affinities. Emission from TAB3 is strongly quenched by the NPs, but not completely. Experiments on living human cells revealed that neither free NPs, nor their composites with TAB3, were toxic. Bioimaging studies by confocal microscopy revealed that all NPs efficiently enter living cells within 90 min. Co-localization experiment with simultaneous collection of data in the reflection

and fluorescence modes demonstrated that the TAB3 dye remained bound to NPs inside cells. Strong irradiation of TAB3-NP inside cells with a 457 nm laser did not yield any damage to the cells, at variance with our previously shown very strong photo-bioactivity of the TAB3 dye alone. Thus, binding of a chromophore to a nanoparticle can inhibit the chromophore's ability to undergo photo-induced singlet oxygen production, consequently blocking its photo-bioactivity.

INTRODUCTION

The potential application of metal nanoparticles (NPs) is indeed broad, including fields such as catalysis, photonics, optoelectronics, surface-enhanced Raman scattering (SERS) (1) to applications in biomedicine, such as anticancer therapy (2), drug delivery (3,4), cell labeling, non-invasive diagnostics (bioimaging and MR imaging), (5–8) and cosmetics (9). The most commonly researched nanoparticles for biomedical purposes are silver nanoparticles (AgNP) due to their previously known antibacterial efficacy (10), and gold nanoparticles (AuNP). Their biological activity, cellular uptake, as well as their toxicity highly depends on their physicochemical characteristics, i.e., their size (11), shape (12), surface charge/coating (13) as well as on the interaction of various nanoparticles (including gold NPs) with physiological fluids (14).

Enea *et al.* (15) investigated the influence of size, capping agent, and the shape of AuNP on cellular uptake and cytotoxicity in two different hepatic cell models. They showed that, in general, AuNPs have a low toxicity towards hepatic cells. However, they demonstrated that the cellular uptake depended significantly on the type of hepatic cells, with smaller AuNPs being more toxic than the larger ones (~15 nm vs 60 nm) and their cellular uptake was higher. Furthermore, citrate-coated NPs showed higher toxicity than 11-mercaptoundecanoic acid-coated ones, and cellular uptake for 60 nm nanostars was higher than that of nanospheres of the same size. Many experimental data showed a similar trend for AgNPs (16,17).

The increased cellular uptake and cytotoxicity of smaller NPs could be explained by their higher probab-

ity of interaction with the biological medium due to their larger specific surface area, i.e., more atoms are on the surface of the NPs (18). The charge, solubility, and biocompatibility of NPs is defined by their coating. In general, positively charged NPs have a longer lifetime in the blood stream compared to negatively charged ones, making them more suitable for drug-delivery purposes (19). Also, their tendency to agglomerate in interactions with a biological medium is well known to affect cellular uptake and cytotoxicity (20). Some nanoparticles also show outer stimuli-induced drug-release (21) or, in particular, photo-induced bioactivity (photo-thermal induced therapy) (22).

We recently reported diethynylarene-linked bis(triarylborane) tetracations for dual fluorimetric and Raman-SERS (SERS = surface-enhanced Raman scattering) sensing of biomacromolecules (23) and promising photodynamic therapy (PDT)-based biological activity on human cell lines and adenovirus type 5 (HAdV5), thus acting as theranostic agents (24). Among these, TAB3 dye (Figure 1A and 1B) excelled in intracellular properties: fluorimetric staining of several organelles and consequent photo-induced bioactivity, as well as in Raman (SERS) signal amplification of the TAB3 dye in a cuvette caused by binding to silver nanoparticles (23). However, these silver-nanoparticle/TAB3 dye composites were not studied in biological systems.

For that reason, questions arose as to whether different types of metal nanoparticles (Au- or Ag-based) with different coatings (negatively charged citrate or neutral PVP) could be efficiently stained by our TAB3 dye in a cuvette. If yes, such novel nanoparticle/TAB3 dye composites could show intriguing cellular activity, both in the dark and under visible light irradiation.

The aim of this research was to screen several Au- and Ag-based nanoparticles of similar size (20–25 nm), differing in their coating (citrate vs PVP), for their cellular uptake, cytotoxicity in the dark and under visible light-irradiation. Furthermore, interactions of these Au- and Ag-based nanoparticles with our very recently developed photo-active fluorophore TAB3 were characterized, and

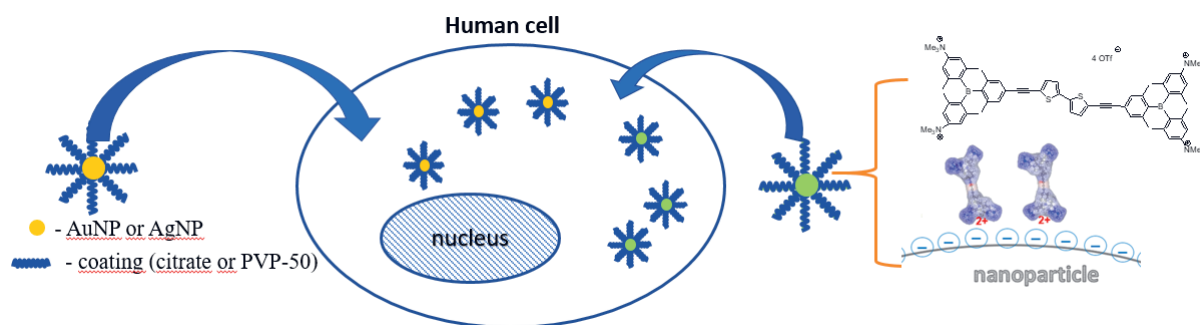


Figure 1. A) Au or Ag nanoparticles studied with various coatings; B) schematic presentation of TAB3 dye binding to a nanoparticle surface (23); C) study of intracellular uptake of the free nanoparticles (A) and the same nanoparticles stained with the TAB3 dye (B).

novel nanoparticle-dye composites were also studied in cells assessing their intracellular staining, eventual photo-induced release, and biological action.

MATERIALS AND METHODS

Synthesis of NPs

Materials

Tetrachloroauric(III) acid trihydrate ($\text{HAuCl}_4 \cdot 3\text{H}_2\text{O}$, $\geq 99,9\%$ trace metal basis), trisodium citrate dihydrate ($\text{C}_6\text{H}_5\text{Na}_3\text{O}_7 \cdot 2\text{H}_2\text{O}$, puriss, p.a., ASC reagent, $\geq 99,0\%$) and polyvinylpyrrolidone (PVP-50, $(\text{C}_6\text{H}_9\text{NO})_n$, powder, $M_w \approx 50000$) were purchased from Sigma-Aldrich. Tannic acid ($\text{C}_{76}\text{H}_{52}\text{O}_{46}$, puriss) and silver nitrate (AgNO_3 , ASC reagent, $\geq 99,0\%$) were purchased from Honeywell, Fluka. Sodium cacodylate trihydrate (sodium cacodylate, $\text{Na}(\text{CH}_3)_2\text{AsO} \cdot 3\text{H}_2\text{O}$, 98%) for buffer preparation was purchased from Alfa Aesar. Nitric acid (HNO_3 , 65%, p.a.) was purchased from KEFO and hydrochloric acid (HCl , 37%) from GramMol. All chemicals were used without further purification. For preparation of aqueous solutions, as well as for synthesis of NPs, Milli-Q Water (MQW) was used. For buffered aqueous solutions, sodium cacodylate buffer, $\text{pH} = 7.0$, $I = 0.05 \text{ M}$ was used. Dye TAB3 used for staining nanoparticles was prepared as described previously (23).

Methods

For all protocols for the synthesis of nanoparticles, all glassware used in the experiments was cleaned with freshly prepared aqua regia ($\text{HCl}:\text{HNO}_3$ volume ratio = 3:1), rinsed thoroughly in ultrapure water, and dried under nitrogen prior to use.

UV-Vis measurements were performed on a Varian Cary 100 Bio spectrophotometer (Agilent Technologies) and fluorescence measurements were performed on a Cary Eclipse fluorescence spectrophotometer (Agilent Technologies). Resulting titration data were fitted with an exponential function obtaining $R^2 > 0.99$ in all cases. All measurements were performed in 10 mm x 10 mm cuvettes at room temperature (25 °C).

Scanning electron microscopy (SEM) measurements were carried out in order to determine the morphology and size of the nanoparticles. Plain view images were taken using a field-emission microscope Jeol JSM 7000F at an acceleration voltage of 1 kV. SEM samples were prepared by depositing a drop of a diluted nanoparticle suspension onto a silicon wafer and air-drying at room temperature. SEM images were analyzed using ImageJ software (25) and the average diameter of the nanoparticles was obtained from the analysis.

Synthesis of gold nanoparticles

Citrate-coated gold nanoparticles (AuNP/cit) were synthesized following the previously published two-step

procedure (synthesis of Au seeds and then immediate growth of the seeds) (26) with minor modification. In a three-neck round bottomed flask, 50 mL of an aqueous 2.2 mM sodium citrate solution was heated to a boil. A condenser, attached to the flask, was used to prevent the evaporation of the solvent. After 3 min of boiling, 400 μL of 25 mM HAuCl_4 was injected into the solution. The color of the solution changed quickly from yellow to blueish-grey and then to pink within 10 min, when the Au seeds were formed. After seed formation, the reaction was cooled to 85 °C. The growth of AuNPs occurred immediately after the seed formation, in the same flask. After cooling to 85 °C, 400 μL of 25 mM HAuCl_4 was injected into the reaction. After 25 min, after the first growing step was finished, an additional 400 μL of 25 mM HAuCl_4 was injected into the reaction mixture. When the second growing step was complete (after 25 min), the reaction was cooled to room temperature. To remove excess trisodium citrate salt, the AuNPs obtained were centrifuged at 12 000 x g for 10 min and then dispersed in ultrapure water. The molar concentration of the AuNPs was calculated from a UV-Vis spectrum using extinction coefficients obtained from Mie theory calculations for citrate-coated spherical Au nanoparticles (27).

Synthesis of silver nanoparticles

Silver nanoparticles were synthesized using both trisodium citrate and tannic acid as reducing agents according to a published protocol (28). Briefly, in a three-neck round bottomed flask, 50 mL of a solution containing 5 mM trisodium citrate and 0.1 mM tannic acid was heated to a boil. A condenser, attached to the flask, was used to prevent the evaporation of the solvent. After 3 min of boiling, 500 μL of 25 mM AgNO_3 was injected into the solution. The solution immediately changed color to bright yellow. After 25 min, the reaction was complete and was cooled to room temperature. To remove tannic acid and excess trisodium citrate salt, the AgNPs obtained were centrifuged at 12 000 x g for 10 min and then dispersed in ultrapure water. The molar concentration of citrate stabilized Ag nanoparticles was calculated from UV-Vis spectrum using experimentally obtained extinction coefficient data for citrate stabilized spherical silver nanoparticles (29).

Preparation of PVP-coated NPs

PVP-coated gold and silver nanoparticles were prepared by adding 500 μL of 1 mM PVP-50 into 1 mL of a suspension of the nanoparticles. After 12 h of incubation, the solution was centrifuged once at 12 000 x g for 10 min and the nanoparticles were dispersed in sodium cacodylate buffer solution ($I = 0.05 \text{ M}$; $\text{pH} = 7.0$).

The concentration of the stock solutions for both citrate- and PVP-50-coated AuNPs (AuNP/cit and AuNP/PVP-50, respectively, in further text) suspensions were adjusted to be $5 \times 10^{-10} \text{ M}$ and for AgNP suspensions

(both AgNP/cit and AgNP/PVP-50) to be 5×10^{-11} M (by centrifugation of the suspension and then by dilution with either ultrapure water or sodium cacodylate buffer solution) for further purposes.

Determination of binding constants of TAB3 with nanoparticles

The binding constant of TAB3 with nanoparticles was determined by fluorimetric titration of TAB3 ($c = 2.1 \times 10^{-7}$ M) in water or sodium cacodylate buffer ($pH = 7.0$, $I = 0.05$ M) by adding aliquots of NPs' suspensions. For titration purposes, the concentration of the stock solution of AuNP (PVP-50 and citrate coated) was 5×10^{-10} M and that of AgNP was 5×10^{-11} M. The quenching of emission of TAB3 was recorded at 531 nm (in experiments with AgNPs) and 522 nm (for AuNPs) after excitation at 413 nm. Titration data were fitted in Origin 7.0 software to the first exponential equation, giving apparent binding constants (K_{app}).

Biology

Cells

A549 cells (human lung carcinoma; ATCC CCL-185) were obtained from the ATCC Cell Biology Collection and were cultured according to the manufacturer's instructions. Cells were grown in Dulbecco Modified Eagle's Medium (DMEM, Sigma Aldrich, USA) supplemented with 10% of fetal bovine serum (FBS, Sigma Aldrich, USA) at 37 °C and 5% CO₂ in a humidified atmosphere.

Cytotoxicity assay – MTT

Cells were seeded on 96 well plates at concentrations of 7×10^3 cells/well in 100 µL of DMEM (10% FBS) and left in the incubator overnight (37 °C, 5% CO₂). The next day, 100 µL of the working solution of the samples was added to the wells, thus the final volume was 200 µL/well. The stock solutions used for antiproliferative screening were 3.5×10^{-2} M for AuNPs and 4×10^{-10} M for AgNPs. The concentrations tested were $3.5 \times 10^{-10} - 3.5 \times 10^{-12}$ for AuNPs and $4 \times 10^{-11} - 4 \times 10^{-13}$ M for AgNPs. All measurements were made in quadruplicate. The plates were then incubated for the next 72 h (37 °C, 5% CO₂). After incubation, the medium was removed, and 40 µL of an MTT solution was added to each well. The plates were incubated in the cell incubator for 3 h, allowing formazan crystals to form. After 3 h, 170 µL of DMSO was added to each well and the plates were placed on a shaker for 20 min, allowing the crystals to dissolve. The absorbance of the MTT-formazan product was measured with a microplate reader at 600 nm, and the absorbance value correlates directly with cell survival. For irradiation experiments, cell culture plates, prepared as above, were treated with the compounds studied, incubated for 90 min (37 °C, 5% CO₂) in order to allow the compounds to enter the cells, and irradiated in a Luzchem reactor with

UV light, 350 nm, 8 lamps, in total 8 W, dose 50.6 mw* m^{-2} ; ~18 cm lamp to cell-plate). Irradiation for 10 min and 30 min per day was performed on three consecutive days at the same times each day.

Live cell imaging

Live imaging of the cells treated with the compounds was performed on the A549 cell line. Cells were seeded in Ibidi imaging cell chambers (Ibidi®, Germany) in 500 µL of medium, with a concentration of 5×10^4 cells/well and left in the cell incubator for 48 h (37 °C, 5% CO₂). After two days, cells were treated with a 1×10^{-11} M solution of the NP system to be tested and left in the cell incubator for 90 min or overnight to allow the compound to enter the cells. Then, the cells were rinsed and observed using a Leica SP8 X confocal microscope (Leica Microsystems, Germany) with a 63 x/1.40 oil-immersion objective for imaging, using the 457 nm laser and operating in the reflection mode to collect Reflection Interference Contrast Microscopy (RICM) images, or in the fluorescence mode to collect emission images (only in the presence of the TAB3 dye). The images were analyzed using LAS X (Leica Microsystems, Germany) and ImageJ (NIH, USA) software and they show maximum projections of confocal stacks, unless otherwise indicated.

RESULTS AND DISCUSSION

Studies in aqueous solutions (cuvette)

Characterization of gold and silver nanoparticles

As the cellular uptake depends on the size and shape of the nanoparticles, citrate-coated gold and silver nanoparticles were characterized by UV-Vis spectroscopy and SEM.

Figure 2A shows typical UV-Vis spectra of AgNP/cit and AuNP/cit in ultrapure water with maximum absorbances of 410 nm and 519 nm, respectively. SEM microscopy (Figure 2B and 2C) showed that both AgNP/cit and AuNP/cit were homogeneous and quasi-spherical in shape, with average diameters of $24.5 \text{ nm} \pm 2.8 \text{ nm}$ and $20.7 \text{ nm} \pm 2.6 \text{ nm}$ (insets in Figure 2B and 2C), respectively. The shape and size of both AgNP/cit and AuNP/cit are in good agreement with results of published protocols (26,28).

Interactions of the TAB3 dye with various NP

Stock solutions of the well-defined AgNPs and AuNPs were then titrated into buffered aqueous solutions of the TAB3 dye, monitoring the change of TAB3 emission (Figures 3 and 4). In general, emission from TAB3 was hypsochromically shifted and strongly quenched, although the extent of quenching was dependent on the type of NP (Table 1; I/I_0). This result suggests that bind-

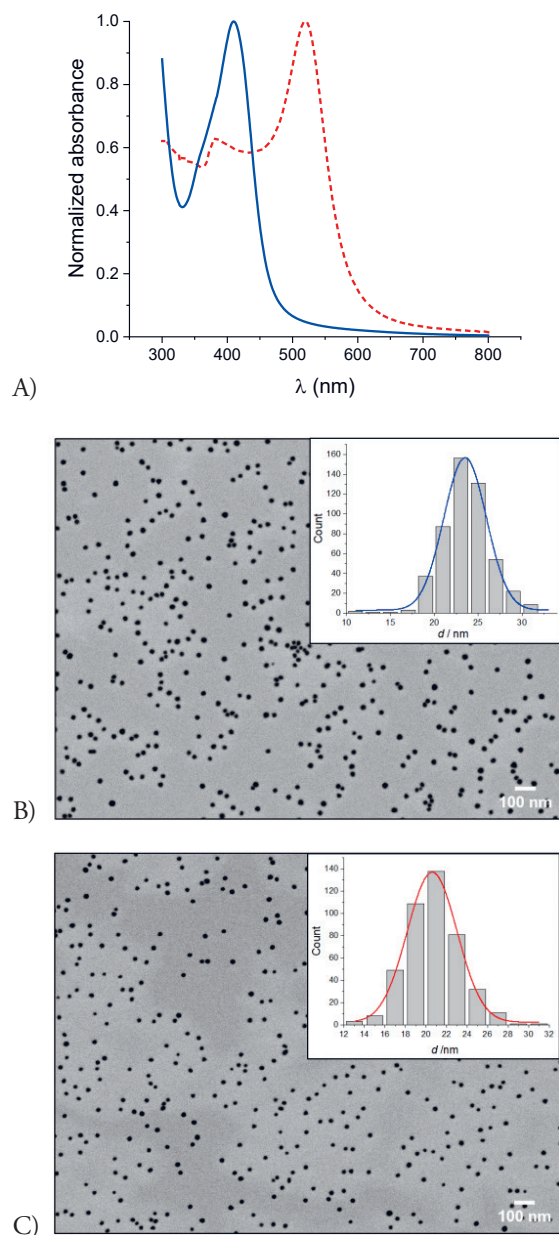


Figure 2. A) UV Vis spectra of AgNP/cit (full blue line) and AuNP/cit (dashed red line); B) SEM image of AgNP/cit with INSET: AgNP/cit diameter distribution; C) SEM image of AuNP/cit with INSET: AuNP/cit diameter distribution.

ing of TAB3 to the nanoparticle surface strongly increased non-radiative relaxation pathways of the chromophore.

Calculation of binding constants which could be attributed to the TAB3-NP complex is quite challenging as it is not possible to determine the exact number of binding sites available on the surface of a particular NP. However, non-covalent equilibrium of the TAB3-NP interaction was very fast (as shown by almost immediate equilibration of emission upon every addition of an NP aliquot during titration), strongly supporting non-covalent interactions.

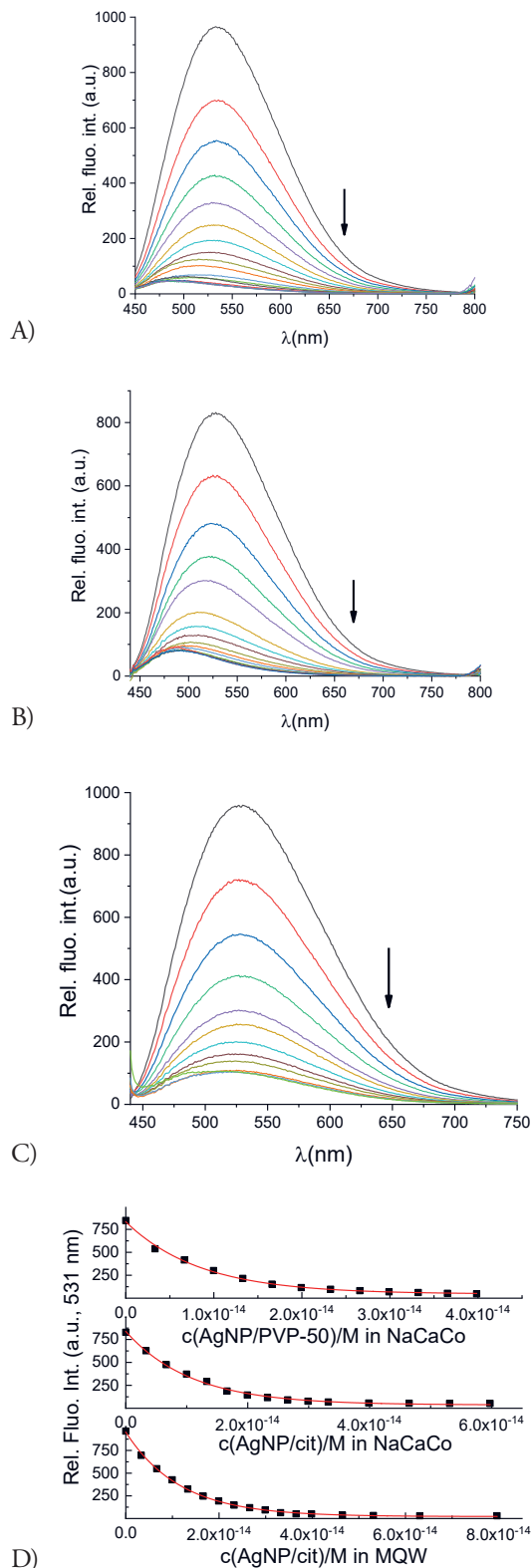


Figure 3. Change in the fluorescence spectrum of TAB3 ($c = 2.1 \times 10^{-7}$, $\lambda_{exc} = 413$ nm) at 298 K upon titration with: A) AgNP/cit in water; B) AgNP/cit in sodium cacodylate buffer; C) AgNP/PVP-50 in sodium cacodylate buffer; D) emission dependence at $\lambda_{max} = 531$ nm of TAB3 on $c(\text{AgNP})$, red line-fit to the 1:1 stoichiometry complex formation.

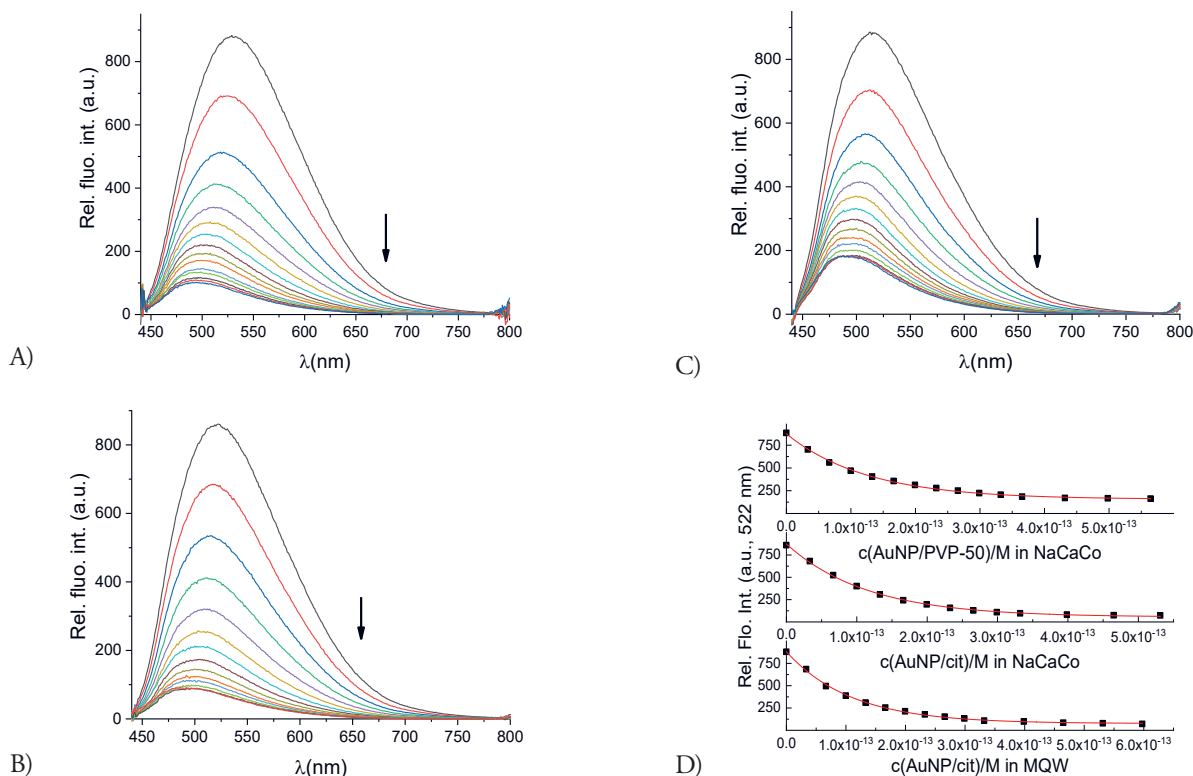


Figure 4. Change in the fluorescence spectrum of TAB3 ($c = 2.1 \times 10^{-7}$ M, $\lambda_{exc} = 413$ nm) at 298 K upon titration with: **A)** AuNP/cit in water; **B)** AuNP/cit in sodium cacodylate buffer; **C)** AuNP/PVP-50 in sodium cacodylate buffer; **D)** emission dependence at $\lambda_{max} = 522$ nm of TAB3 on $c(\text{AuNP})$, red line-fit to the 1:1 stoichiometry complex formation.

Thus, presuming that all TAB3 molecules bind non-cooperatively in the same way, we obtained an excellent fit of the experimental data to the first exponential equation, giving us apparent binding constants (K_{app} ; Table 1). Such K_{app} values do not represent exact binding constants of 1:1 stoichiometry (K_s 1:1), but an estimated K_{app} value which is useful for the determination of the TAB3-NP ratio necessary to have all dye bound to the particular NP, which is essential information for the biological experiments described below. More detailed analysis of K_{app} values revealed that the affinity of TAB3 toward AgNPs is an order of magnitude higher than toward AuNPs. However, coating of particular NP had only a negligible impact on the K_{app} values. It should be stressed that after partial quenching by NPs, TAB3 still emits fluorescence sufficient for imaging studies in cells.

Biology

Antiproliferative screening

In order to study the cytotoxic effect of NPs we determined the survival of A549 cells after exposing them to different concentrations of NPs. The cells were treated with 3.5×10^{-10} M, 3.5×10^{-11} M or 3.5×10^{-12} M solutions of AuNP/cit or AuNP/PVP-50, or 4×10^{-10} M, 4×10^{-11} M or 4×10^{-12} M of AgNP/cit or AgNP/PVP-50, and cell survival was assessed by the MTT assay (Figure 5). Both AuNP/cit and AuNP/PVP-50 showed cytotoxic effects at higher concentrations, namely 3.5×10^{-10} M and 3.5×10^{-11} M. At the lowest concentration, 3.5×10^{-12} M, AuNP/cit or AuNP/PVP-50 did not interfere with cell survival. Ag nanoparticles were toxic only at the highest concentration studied, 4×10^{-10} M. When applied at the

Table 1. Binding constants of TAB3 / NPs =1:1 complexes determined by non-linear fitting.

NPs	^a AgNP/cit	^b AgNP/cit	^b AgNP/PVP-50	^a AuNP/cit	^b AuNP/cit	^b AuNP/PVP-50
K_{app} $\times 10^{12}/\text{M}^{-1}$	86.0 ± 2	93.0 ± 4	118.0 ± 5	9.0 ± 0.2	9.0 ± 0.2	8.0 ± 0.2
III_0	0.030	0.064	0.056	0.082	0.085	0.184

^aMilli-Q Water (MQW); ^bSodium cacodylate buffer pH = 7.0, $I = 0.05$ M.

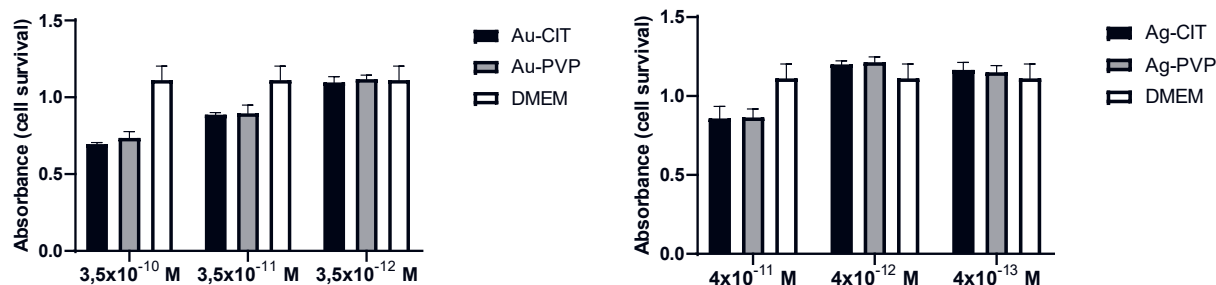


Figure 5. Cell survival of A549 cells incubated with different concentrations of AuNP/cit, AuNP/PVP-50, AgNP/cit and AgNP/PVP-50. Data are presented as mean \pm SD made in four replicates, relative to the control samples. Control samples are cells incubated with cell culture medium (DMEM) alone. Representative data from two independent experiments which yielded similar results are shown.

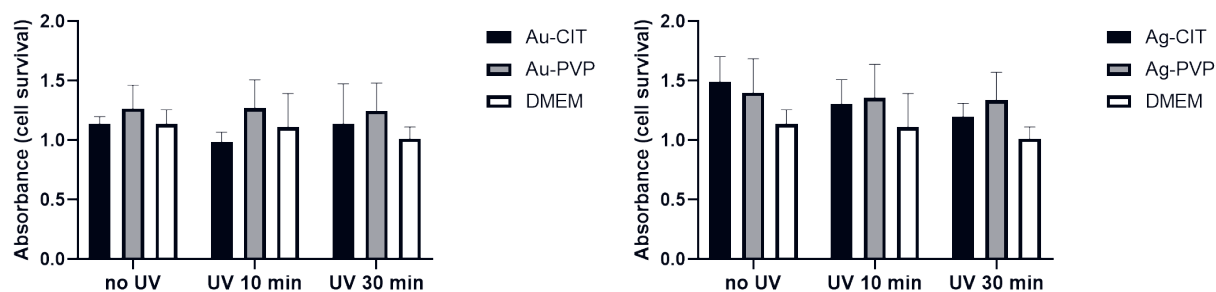


Figure 6. Cell survival of A549 cells incubated with 3.5×10^{-12} M AuNP/cit or AuNP/PVP-50, or 4×10^{-12} M AgNP/cit or AgNP/PVP-50, with or without visible light irradiation. Data are presented as mean \pm SD made in four replicates, relative to the control samples. Control samples are cells incubated with cell culture medium (DMEM) alone. Representative data from three independent experiments which yielded similar results are shown.

lower concentration, neither AgNP/cit nor AgNP/PVP-50 were toxic to the A549 cells. The effect of nanoparticles on cell survival was tested also after exposure to UV light. Regardless of the exposure to UV light, both Au- and Ag-based nanoparticles remained non-toxic at the picomolar concentration range (3.5×10^{-12} M for Au nanoparticles and 4×10^{-12} M for Ag nanoparticles) (Figure 6).

Live cell imaging

To determine whether non-toxicity is a result of non-efficient cellular uptake, we performed live cell imaging experiments on A549 cells treated with AuNP/cit, AgNP/cit or AgNP/PVP-50, all at a concentration of 1×10^{-11} M, using a Leica TCS SP8 X confocal laser scanning microscope (Leica Microsystems) equipped with an HC PL APO CS2 63 \times /1.40 oil objective, using the 457 nm laser and operating in reflection mode.

We used two different incubation times upon addition of nanoparticles to cells (90 min and overnight – 16 h) and, under both conditions, all nanoparticles studied efficiently entered cells, as clearly demonstrated in reflection mode images (Figure 7) in comparison to reference experiments performed on cells not treated with NPs (Supporting Information Fig S1).

To confirm the presence of nanoparticles in the cells, we stained AgNP/cit nanoparticles with TAB3 according

to the above determined binding constants (Table 1), i.e., with $c(\text{TAB3}) = 1 \mu\text{M}$, and then incubated the cells with NP/TAB3 for 90 min.

Confocal microscopy experiments in fluorescence mode using the excitation wavelength of the TAB3 dye (457 nm), revealed efficient cellular uptake and significant co-localization (Pearson's coefficient $r = 0.808$) of TAB3 emission (Figure 8B, green) with simultaneous microscopy analysis of the same sample in reflection mode (Figure 8A and 8C). It should be noted that while monitoring the sample in Figure 8 in real time, we noticed that dots attributed to the NPs move, the intensity of movement being proportional to the intensity of laser irradiation. This effect can be attributed to photo-induced heating of the metal NPs. This movement, even at low laser power, interfered to a minor extent with the collection of subsequent images in reflection and fluorescence modes, thus resulting in a bit less than 100% co-localization (Figure 8D).

We recently reported that the TAB3 dye, under intense irradiation at 457 nm for only 1 min, causes severe cellular damage due to singlet oxygen production (24), demonstrated by the confocal microscope movie in the Supp. Info. to ref. 24. Thus, we irradiated TAB3-AuNP/cit composites in cells under the same conditions, but no visible toxicity or cellular damage was observed (data not shown,

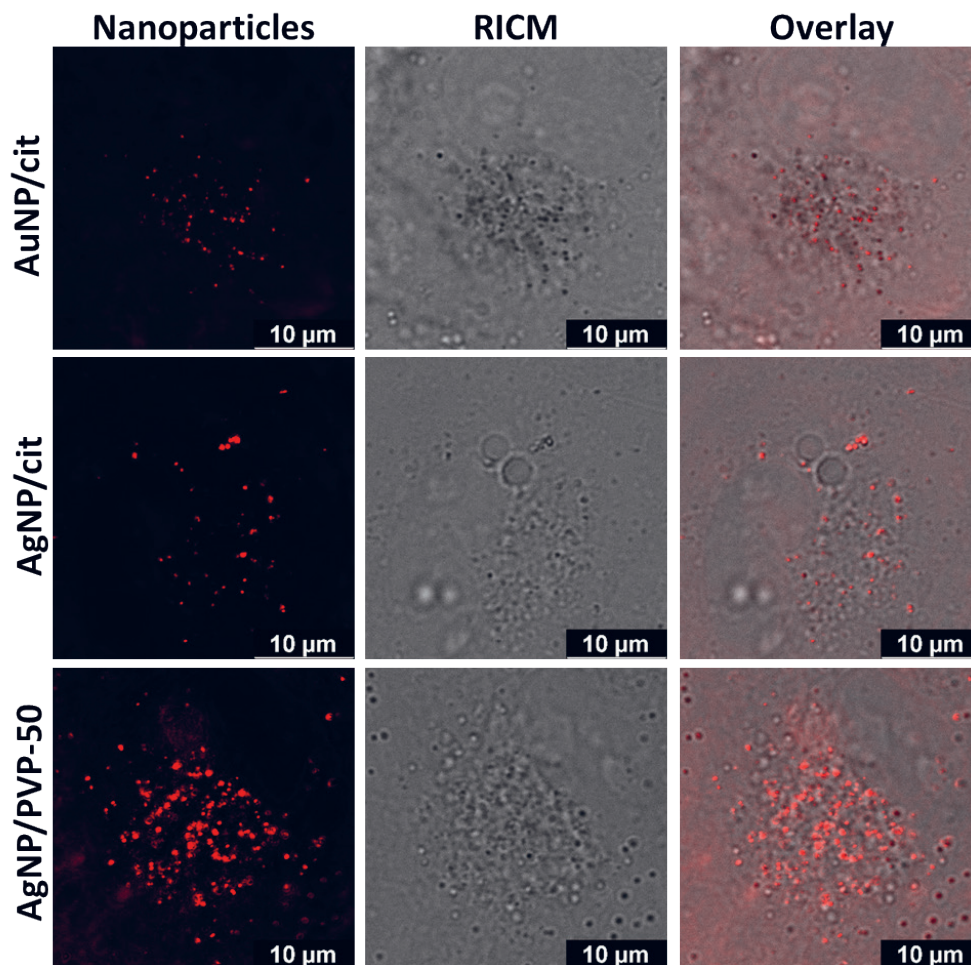


Figure 7. Uptake and localization of AuNP/cit, AgNP/cit and AgNP/PVP-50 in live A549 cells. Cells were incubated with studied compounds overnight (16h) in concentration of 1×10^{-11} M (shown in red; $\lambda_{exc} = 405$ nm). Reflection Interference Contrast Microscopy (RICM) is shown in grey.

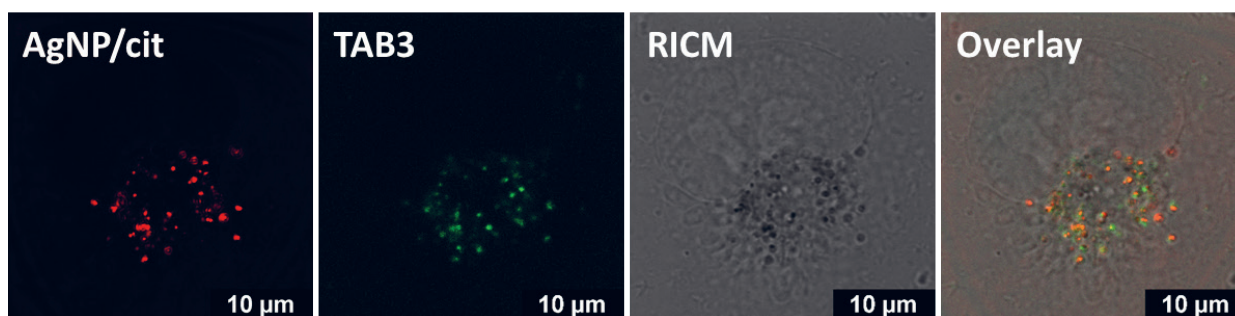


Figure 8. Uptake and localization of AgNP/cit coupled to TAB3 in live A549 cells. Cells were incubated with AgNP/cit in concentration of 1×10^{-11} M (A) shown in red) and TAB3 at a concentration of $1 \mu\text{M}$ (B) shown in green) for 90 min. Reflection Interference Contrast Microscopy (RICM) is shown in grey (C) and overlay of a,b,c given in (D).

movie available on request). Also, Figure 6 showed that irradiation of cells treated with TAB3-NP in a photochemical reactor for even 30 min did not produce a measurable cytotoxic effect, at variance to the results for TAB3-treated cells (24), where, under the same conditions, all cells were killed.

This result could be correlated with the TAB3 emission quenching upon binding to NPs (Figures 3, 4 and Table 1), attributed to the enhanced non-radiative decay of the fluorophore caused by the metal nanoparticle surface. We showed above, in co-localization experiment in reflection and fluorescence modes, that TAB3 remained bound to

NPs in a cellular environment. As singlet oxygen production by TAB3 is directly related to intersystem crossing (ISC) from singlet to triplet excited state (24), which takes place on a timescale roughly similar to that of fluorescence, NP-caused fluorescence quenching by enhanced non-radiative decay rates will also likely interfere with ISC by providing another competing pathway for deactivation of the S_1 state, while those molecules which did undergo ISC to the triplet state might also undergo enhanced non-radiative decay, both of which would result in diminishing the photo-induced bioactivity.

CONCLUSIONS

Au and Ag nanoparticles (NPs) were non-covalently stained by the fluorescent dye TAB3 irrespective of the different coatings (negatively charged citrate or neutral PVP) with similar binding affinities. Emission from TAB3 is strongly quenched by the NPs, but not completely; thus, the remaining emission allowed monitoring of stained TAB3-NP in biological systems.

Experiments on living human cells (A549) revealed that neither free NPs, nor their composites with TAB3, were toxic. Bioimaging studies by confocal microscopy, performed in the reflection mode and also in the fluorescence mode with TAB3-stained NPs, revealed that all NPs efficiently enter living cells within 90 min. Co-localization experiment with simultaneous collection of data in the reflection and fluorescence modes demonstrated that the TAB3 dye remained bound to NPs inside cells.

However, strong irradiation of TAB3-NP inside cells with a 457 nm laser did not yield any damage to the cells, at variance with our previously shown very strong photo-bioactivity of the TAB3 dye alone (24). Thus, binding of a chromophore to a nanoparticle can inhibit the chromophore's ability to undergo photo-induced singlet oxygen production, consequently blocking its photo-bioactivity. This finding can be applied in two ways: either for suppressing harmful effects of photo-active chromophores or for the design of novel photodynamic therapy (PDT) systems. The later PDT-composites would be based on non-active PDT-drug/NP composites which efficiently enter living cell, and, inside the cells, the PDT drug would be released by internal or external stimuli, thus becoming photo-bioactive.

Acknowledgements: *The financial support of the Croatian Science Foundation project IP-2018-01-5475 and HRZZ-IP-2019-04-6048, the DAAD, and the Julius-Maximilians-Universität Würzburg are gratefully acknowledged.*

REFERENCES

- MORAN CH, XIA Y 2012 Controlling the Synthesis and Assembly of Silver Nanocrystals for Single-Molecule Detection by SERS. *Proc. of SPIE* 8373: 837321–6. <https://doi.org/10.1117/12.919380>
- ZHANG X-F, LIU Z-G, SHEN W, GURUNATHAN S 2016 Silver Nanoparticles: Synthesis, Characterization, Properties, Applications, and Therapeutic Approaches. *Int. J. Mol. Sci.* 17: 1534. <https://doi.org/10.3390/ijms17091534>
- DREADEN EC, ALKILANY AM, HUANG X, MURPHY CJ, EL-SAYED MA 2012 The Golden Age: Gold Nanoparticles for Biomedicine. *Chem. Soc. Rev.* 41: 2740–79. <https://doi.org/10.1039/C1CS15237H>
- IVANOVA N, GUGLEVA V, DOBREVA M, PEHLIVANOV I, STEFANOV S, ANDONOVA V 2019 Silver Nanoparticles as Multi-Functional Drug Delivery Systems. *Nanomedicines*, edited by Farrukh MA. IntechOpen. <https://doi.org/10.5772/intechopen.80238>
- IV M, TELISCHAK N, FENG D, HOLDSWORTH SJ, YEOM KW, DALDRUP-LINK HE 2015 Clinical applications of iron oxide nanoparticles for magnetic resonance imaging of brain tumors. *Nanomedicine* 10: 993–1018. <https://doi.org/10.2217/nmm.14.203>
- AUSTIN LA, MACKAY MA, DREADEN EC, EL-SAYED MA 2014 The Optical, Photothermal, and Facile Surface Chemical Properties of Gold and Silver Nanoparticles in Biodiagnostics, Therapy, and Drug Delivery. *Arch. Toxicol.* 88: 1391–1417. <https://doi.org/10.1007/s00204-014-1245-3>
- BETZER O, MEIR R, DREIFUSS T, SHAMALOV K, MOTIEI M, SHWARTZ A, BARANES K *et al.* 2015 In-Vitro Optimization of Nanoparticle-Cell Labeling Protocols for In-Vivo Cell Tracking Applications. *Sci. Rep.* 5: 15400. <https://doi.org/10.1038/srep15400>
- PANZARINI E, MARIANO S, CARATA E, MURA F, ROSSI M, DINI L 2018 Intracellular Transport of Silver and Gold Nanoparticles and Biological Responses: An Update. *Int. J. Mol. Sci.* 19: 1305. <https://doi.org/10.3390/ijms19051305>
- WIECHERS JW, MUSEE N 2010 Engineered Inorganic Nanoparticles and Cosmetics: Facts, Issues, Knowledge Gaps and Challenges. *J. Biomed. Nanotech.* 6: 408–31. <https://doi.org/10.1166/jbn.2010.1143>
- KUNG J-C, WANG W-H, LEE C-L, HSIEH H-C, SHIH C-J 2020 Antibacterial Activity of Silver Nanoparticles (AgNP) Confined to Mesoporous, Silica-Based Calcium Phosphate against Methicillin-Resistant Staphylococcus Aureus (MRSA). *Nanomaterials* 10: 1264. <https://doi.org/10.3390/nano10071264>
- WU M, GUO H, LIU L, LIU Y, XIE L 2019 Size-Dependent Cellular Uptake and Localization Profiles of Silver Nanoparticles. *Int. J. Nanomedicine* 14: 4247–59. <https://doi.org/10.2147/IJN.S201107>
- XIE X, LIAO J, SHAO X, LI Q, LIN Y 2017 The Effect of Shape on Cellular Uptake of Gold Nanoparticles in the Forms of Stars, Rods, and Triangles. *Sci. Rep.* 7: 3827. <https://doi.org/10.1038/s41598-017-04229-z>
- CHO EC, ZHANG Q, XIA Y 2011 The Effect of Sedimentation and Diffusion on Cellular Uptake of Gold Nanoparticles. *Nat. Nanotechnol.* 6: 385–91. <https://doi.org/10.1038/nnano.2011.58>
- ALKILANY AM, MURPHY CJ 2010 Toxicity and Cellular Uptake of Gold Nanoparticles: What We Have Learned so Far? *J. Nanopart. Res.* 12: 2313–33. <https://doi.org/10.1007/s11051-010-9911-8>
- ENE A M, PEREIRA E, COSTA J, SOARES ME, DIAS DA SILVA D, BASTOS ML, CARMO HF 2021 Cellular Uptake and Toxicity of Gold Nanoparticles on Two Distinct Hepatic Cell Models. *Toxicol. in Vitro* 70: 105046. <https://doi.org/10.1016/j.tiv.2020.105046>
- GLIGA AR, SKOGLUND S, ODNEVALL WALLINDER I, FADEEL B, KARLSSON HL 2014 Size-Dependent Cytotoxicity of Silver Nanoparticles in Human Lung Cells: The Role of Cellular Uptake, Agglomeration and Ag Release. *Part. Fibre Toxicol.* 11: 11. <https://doi.org/10.1186/1743-8977-11-11>

17. CABALLERO-DIAZ E, PFEIFFER C, KASTL L, RIVERA-GIL P, SIMONET B, VALCÁRCEL M, JIMÉNEZ-LAMANA J, LABORDA F, PARAK WJ 2013 The Toxicity of Silver Nanoparticles Depends on Their Uptake by Cells and Thus on Their Surface Chemistry. *Part. Part. Syst. Charact.* 30: 1079–85. <https://doi.org/10.1002/ppsc.201300215>
18. BAKAND S, HAYES A 2016 Toxicological Considerations, Toxicity Assessment, and Risk Management of Inhaled Nanoparticles. *Int. J. Mol. Sci.* 17: 929. <https://doi.org/10.3390/ijms17060929>
19. ZHANG X-F, LIU Z-G, SHEN W, GURUNATHAN S 2016 Silver Nanoparticles: Synthesis, Characterization, Properties, Applications, and Therapeutic Approaches. *Int. J. Mol. Sci.* 17: 1534. <https://doi.org/10.3390/ijms17091534>
20. LANKOFF A, SANDBERG WJ, WEGIEREK-CIUK A, LISOWSKA H, REFSNES M, SARTOWSKA B, SCHWARZE PE, MECZYNSKA-WIELGOSZ S, WOJEWODZKA M, KRUSZEWSKI M 2012 The Effect of Agglomeration State of Silver and Titanium Dioxide Nanoparticles on Cellular Response of HepG2, A549 and THP-1 Cells. *Toxicol. Lett.* 208: 197–213. <https://doi.org/10.1016/j.toxlet.2011.11.006>
21. AZNAR E, OROVAL M, PASCUAL L, MURGUIA JR, MARTINEZ-MANEZ R, SANCENON F 2016 Gated Materials for On-Command Release of Guest Molecules. *Chem. Rev.* 116: 561–718. <https://doi.org/10.1021/acs.chemrev.5b00456>
22. KANG B, AFIFI MM, AUSTIN L A, EL-SAYED MA 2013 Exploiting the Nanoparticle Plasmon Effect: Observing Drug Delivery Dynamics in Single Cells via Raman/Fluorescence Imaging Spectroscopy. *ACS Nano* 7: 7420–7427. <https://doi.org/10.1021/nn403351z>
23. FERGER M, BAN Z, KROSLI I, TOMIC S, DIETRICH L, LORENZEN S, RAUCH F, SIEH D, FRIEDRICH A, GRIESBECK S, KENDEL A, MILJANIC S, PIANTANIDA I, MARDER TB 2021 Bis(phenylethynyl)arene Linkers in Tetracationic Bis-triarylborane Chromophores Control Fluorimetric and Raman Sensing of Various DNAs and RNAs. *Chem.Eur.J.* 27: 5142–5159. <https://doi.org/10.1002/chem.202005141>
24. BOZINOVIC K, NESTIC D, MICHAIL E, FERGER M, KOSCAK M, LAMBERT C, MAJHEN D, MARDER TB, PIANTANIDA I 2022 Diethynylarene-linked bis(triarylborane) cations as theranostic agents for tumor cell and virus-targeted photodynamic therapy. *J. Photochem. Photobiol. B* 234: ARTN 112523. <https://doi.org/10.1016/j.jphotobiol.2022.112523>
25. SCHNEIDER CA, RASBAND WS, ELICEIRI KW 2012 NIH Image to ImageJ: 25 years of image analysis. *Nat. Methods* 9: 671–75. doi:10.1038/nmeth.2089
26. BASTÚS NG, COMENGE J, PUNTES V 2011 Kinetically Controlled Seeded Growth Synthesis of Citrate-Stabilized Gold Nanoparticles of up to 200 nm: Size Focusing versus Ostwald Ripening. *Langmuir* 27: 11098–105. <https://doi.org/10.1021/la201938u>
27. HAISS W, THANH NTK, AVEYARD J, FERNIG DG 2007 Determination of Size and Concentration of Gold Nanoparticles from UV-Vis Spectra. *Anal. Chem.* 79: 4215–21. <https://doi.org/10.1021/ac0702084>
28. BASTÚS NG, MERKOÇI F, PIELLA J, PUNTES V 2014 Synthesis of Highly Monodisperse Citrate-Stabilized Silver Nanoparticles of up to 200 nm: Kinetic Control and Catalytic Properties. *Chem. Mater.* 26: 2836–46. <https://doi.org/10.1021/cm500316k>
29. PARAMELLE D, SADOVOY A, GORELIK S, FREE P, HOBLEY J, FERNIG DG 2014 A Rapid Method to Estimate the Concentration of Citrate Capped Silver Nanoparticles from UV-Visible Light Spectra. *The Analyst* 139: 4855–61. <https://doi.org/10.1039/C4AN00978A>